Electrospun Fibrous Mats with High Porosity as Potential Scaffolds for Skin Tissue Engineering

Xinli Zhu,[†,‡] Wenguo Cui,[†] Xiaohong Li,[*,†] and Yan Jin[*,‡]

Key Laboratory of Advanced Technologies of Materials, Ministry of Education, School of Materials Science and Engineering, Southwest Jiaotong University, Chengdu 610031, People's Republic of China, and Research and Development Center for Tissue Engineering, College of Stomatology, Fourth Military Medical University, Xi'an 710032, People's Republic of China

Received January 6, 2008; Revised Manuscript Received May 25, 2008

Diffusional limitations of mass transport have adverse effects on engineering tissues that normally have high vascularity and cellularity. The current electrospinning method is not always successful to create micropores to encourage cell infiltration within the scaffold, especially when relatively large-sized pores are required. In this study, a slow rotating frame cylinder was developed as the collector to extend the pore size and increase the porosity of electrospun fibrous scaffolds. Fibrous mats with porosity as high as 92.4% and average pore size of 132.7 μm were obtained. Human dermal fibroblasts (HDFs) were seeded onto these mats, which were fixed on a cell-culture ring to prevent the shrinkage and contraction during the incubation. The viability test indicated that significantly more HDFs were generated on highly porous fibrous mats. Toluidine blue staining showed that the highly porous scaffold provided mechanical support for cells to maintain uniform distribution. The cross-section observations indicated that cells migrated and infiltrated more than 100 μm inside highly porous fibrous mats after 5 d incubation. The immunohistochemistry analysis demonstrated that cells began secreting collagen, which is the main constituent of extracellular matrix. It is supposed that highly porous electrospun fibrous scaffolds could be constructed by this elaboration and may be used for skin tissue engineering.

Introduction

Tissue engineering seeks to repair or replace damaged tissue using a combination of cellular/molecular biology and material chemistry/engineering. One of the challenges is the design of reproducible three-dimensional (3D) scaffolds that can mimic the structure and biological functions of the natural extracellular matrix (ECM), which guide the cellular migration, provide mechanical support, and regulate cellular activities. Fibrous mats prepared by an electrospinning technique, with the excellent characteristics such as high surface area to volume ratio and similar structural morphology to the fibrillar ECM, have already shown potential as effective tissue engineering scaffolds.[1,2] These scaffolds have a skeletal structure with individual fiber diameters ranging from a few nanometers to micrometers. Additionally, the scaffold structure changes dynamically over time as the polymer nanofibers degrade, allowing the seeded cells to proliferate and produce their own ECM.[3] Electrospun nano- to microfibers have been investigated as scaffolds for engineering tissues such as cartilages, bones, arterial blood vessels, heart, and nerves.[4–7]

Diffusional limitations have severely hampered mass transport for engineering tissues that normally have high vascularity and cellularity. Establishing a cell-populated 3D scaffold requires cell migration into the scaffold structure, not just on the substrate surface. There have been many attempts to make 3D electrospun fibrous scaffolds with controlled pore size, pore geometry, fiber dimension, and spatial orientation.[8] All these features are essential for the transport of oxygen and nutrient supply to the cells and for the cellular growth, leading to tissue regeneration. The pores generated within the electrospun scaffold are formed by nanofibers lying randomly upon each other, which are different from isotropic pores made by using particles or bubbles when a scaffold is solidified.[9] Eichhorn et al.[10] showed that the mean pore radius of electrospun matrices exponentially decreased with fiber size. Individual fiber diameters typically ranged from 50 nm to a few micrometers, which necessarily resulted in fibrous mats containing pores in the similar range of electrospun fibers.[11] Nutrients and metabolic wastes may pass through the nanosized porosity of electrospun mats, but it seems too small to provide enough space for cell ingrowth. Van Lieshout et al. showed poor penetration of human myofibroblasts into electrospun fibrous mat compared to a knitted equivalent.[12] Therefore, there is a need to develop techniques providing relatively large pores within the electrospun fibrous mat, while sustaining the scaffold geometry during cell growth.

A few fabrication techniques have been proposed to control the pore size and increase the porosity of electrospun fibrous scaffolds in a consistent manner. To design a mesoscopically ordered structure of matrices, Kidoaki et al. suggested multilayering electrospinning and mixing electrospinning.[13] To facilitate the infiltration while retaining its extracellular matrix-like character, Nam et al. combined electrospinning with salt leaching to produce a scaffold, which increased the as-spun porosity from 79 (salt-free) to 83% and extended the cellular infiltration of electrospun matrices.[14] Their results indicated that the leaching process did not significantly degrade the fibers, but some slight swelling of the overall structure was observed. Furthermore, the use of salt with the size of 90−106 μm as the porogen did not result in uniform pores within the electrospun fibrous mat due to lack of control of salt placement.

* To whom correspondence should be addressed. Phone: +8628-87634023 (X. L.); +8629-84776147 (Y. J.). Fax: +8628-87634649 (X. L.); +8629-83218039 (Y. J.). xhli@swjtu.edu.cn (X. L.); yanjin@fmmu.edu.cn (Y. J.).

† Southwest Jiaotong University.

‡ Fourth Military Medical University.

10.1021/bm800476u CCC: $40.75
Published on Web 06/26/2008

In addition to enlarging pore size and increasing porosity of electrospun fibrous scaffolds, researchers have made other attempts to enhance cell penetration within electrospun matrices, which mostly depended upon the scaffold material, cell loading, and culture conditions. Chiu et al. demonstrated that inclusion of collagen into poly(L-lactide) (PLLA) nanofibrous scaffolds appeared to facilitate both cell attachment and migration within the scaffold. But for PLLA scaffold, cell migration was no more than 40 μm after a one week culture.[15] Mikos et al. observed infiltration of cells into electrospun poly(ε-caprolactone) scaffolds under flow perfusion culture but not under static condition.[16] Chong et al. performed cell culture on both sides of the nanofibrous scaffold to facilitate cell penetration.[17] Alternatively, dynamic depth filtration has achieved effective seeding in fibrous scaffolds,[18] but the dynamic cell loading and cell culture system would not be as successful in standard electrospun mats, owing to the small pore sizes.[18]

Human dermal fibroblast (HDF, 10−100 μm), the major cell type of the dermis, is essential to ECM deposition and remodeling. Human cells can attach and organize well around fibers with diameters smaller than those of the cells.[19] In this regard, nano to submicro scale fibrous scaffolds can provide an optimal template for HDFs to seed, migrate, and grow. However, it is not always successful for the current electrospinning method to create micropores to encourage the HDF infiltration and extracellular matrix deposition within the scaffold.[17,20] In this study, to extend the pore size and increase the porosity of electrospun fibrous scaffolds, a rotating metal frame cylinder was designed and used as the collector in the electrospinning apparatus. Different rotation speeds were applied to acquire electrospun poly (DL-lactide-glycolide; PLGA) fibrous mats with varied porosities. Before HDF seeding, all the mats were fixed on a cell-culture ring to prevent shrinkage and contraction during incubation. HDFs were cultured on the mats in conventional conditions to observe the cell infiltration, growth and collagen synthesis.

Experimental Section

Materials. PLGA (M_w = 70 kDa, L/G = 75/25, M_w/M_n = 1.38) was synthesized in our laboratory.[21] The molecular weight was determined by gel permeation chromatography (GPC, waters 2695 and 2414, Milford, MA) using polystyrene as a standard. The mobile phase consisted of tetrahydrofuran (THF, Sigma, U.S.A.), using a regularity elution at a flow rate of 1.0 mL/min. All other chemicals and solvents were of reagent grade or better, and purchased from Changzheng Regents Company (Chengdu, China), unless otherwise indicated. Cell medium ingredients were purchased from Invitrogen and Gibco, U.S.A.

Electrospinning. The setup of electrospinning system was performed as described elsewhere.[22] Briefly, the electrospinning apparatus was equipped with a high-voltage statitron (Tianjing High Voltage Power Supply Co., Tianjing, China). The polymer was dissolved in acetone (Sigma, U.S.A.; 20 wt %) and added in a 2 mL glass syringe, which was attached with a clinic-shaped metal capillary with the inner diameter of 0.6 mm. The flow rate of 0.5 mL/h was controlled by a precision pump (Zhejiang University Medical Instrument Company, Hangzhou, China) to maintain a steady flow from the capillary outlet. The electrospun fibers were deposited on grounded aluminum foil fixed on a plate-type collector or a rotating frame cylinder collector consisting of metal struts (Scheme 1). The rotating speed of the cylinder collector was controlled by a stepping motor. Three types of fibrous mats were harvested from these collectors: deposited on the plate (FM-P), acquired on the frame cylinder at the rotation speed of 28 rpm (FM-LR) and 60 rpm (FM-HR). The deposition time was optimized to obtain fibrous mats with the thickness of 250−300 μm. All the nonwoven fibrous mats were vacuum-dried at room temperature for 3 d to completely remove any solvent residue prior to further characterization.

Scheme 1. Electrospinning Apparatus with the Collector of Rotating Frame Cylinder

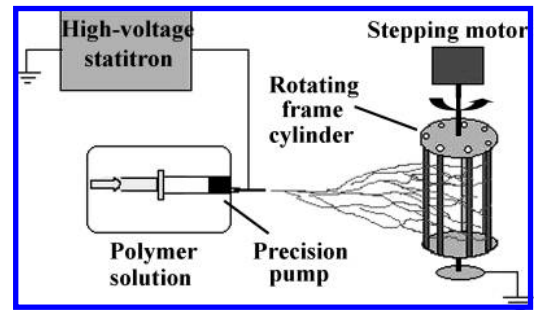

Characterization of Fibrous Mats. The morphologies were observed by scanning electron microscope (SEM, Quanta 200, FEI, The Netherlands) at an accelerating voltage of 20 kV. The fiber diameter was measured from SEM images, and five images were used for each fiber sample. From each image, at least 20 different fibers and 100 different segments were randomly selected and their diameters were measured to generate an average by using Photoshop 8.0 edition.[23] The size of the pores formed between the fibers was measured using ImageJ software version 1.33a. For each sample, at least five SEM images were captured with the magnification of 2,000 from random spots.[24] The apparent density and porosity of electrospun fibrous mats were calculated using the following equations,[25] where the thickness of the fibrous mats was measured by a micrometer.

$$\text{apparent density (g/cm}^3) = \frac{\text{mat mass (g)}}{\text{mat thickness (cm)} \times \text{mat area (cm}^2)}$$

$$\text{mat porosity} = \left(1 - \frac{\text{mat apparent density (g/cm}^3)}{\text{bulk density of PLGA (g/cm}^3)}\right) \times 100\%$$

To clarify the effect of porosity on the mechanical properties of electrospun fibrous mats, tensile tests were conducted following standard mechanical testing methods for fabric materials. The electrospun fibrous mats were punched into small strips (7 × 70 × 0.2 mm^3), and five strips were obtained from different sites of each fibrous sample. The uniaxial tensile properties were characterized using an all-purpose mechanical testing machine (Instron 5567, MA, U.S.A.). The stress−strain curves of the fibrous mats were constructed from the load deformation curves recorded at a stretching speed of 0.5 mm/s. To clarify the effect of porosity on the hydrophilicity of the fibrous mats, a drop of purified water was deposited onto the mat surface using a microsyringe. Solvent-casting film of PLGA was set as control with the thickness of 150 μm. The water contact angles (WCA) of water drops on the electrospun fibrous mat were measured on Kruss GmbH DSA 100 Mk 2 goniometer (Hamburg, Germany) followed by image processing of sessile drop with DSA 1.8 software. The final results were obtained by averaging at least five separate runs.

Culture of HDFs. HDFs were isolated from human foreskins obtained during the circumcision of children by sequential trypsin and collagenase digestion, which were provided by Center for Tissue-Engineering of Fourth military Medical University (Xi'an, China). Fibroblasts of the sixth generation from the same patient were used. These fibroblasts were highly stable, fast growing, and represent well-defined internal cytoskeleton components.[26] About 2 × 10^6 cells were cultured in 75 cm^2 tissue culture plates in Dulbecco's modified Eagle's medium (DMEM; Gibco, U.S.A.) containing 10% fetal bovine serum (FBS, Gibco, U.S.A.), penicillin (100 units/mL), and streptomycin (100 μg/mL) at 37 °C under a humidified atmosphere of 5% CO_2. The culture medium was refreshed every 3 d. When reaching 80−90% confluence, HDFs were trypsinized and subcultivated to fibrous mat samples.

HDF Seeding onto Electrospun Fibrous Mats. Each of the PLGA electrospun fibrous mats of 250−300 μm thickness was cut into small

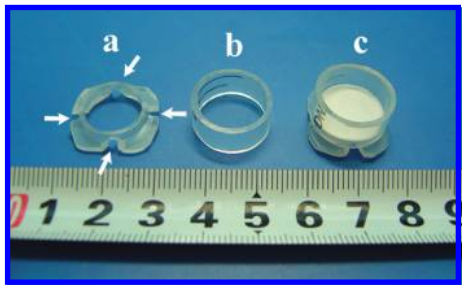

Figure 1. (a) Bottom part with four gaps, indicated as arrows, (b) the upper circle part, and (c) the fibrous mat mounted cell-culture ring.

disks (18−20 mm in diameter). Both sides of the disks were sterilized by ultraviolet irradiation for 2 h and soaked with cell culture medium. To avoid the shrinkage and contraction during incubation, a cell-culture ring made of polystyrene was designed for the current investigation on highly porous fibrous mats. As shown in Figure 1, the fibrous mat was mounted at the bottom part of the cell-culture ring (Figure 1a) before cell seeding and then a plastic ring (Figure 1b) was enclosed on the membrane. Four gaps were made at perpendicular directions at the bottom of the cell-culture ring (Figure 1a), which was aimed to let cell culture medium influent into the space below the fibrous mat and avoid forming air bubbles during cell culture. A total of 50 μL of the HDF suspension (1×10^5 cells/mL) was seeded onto the surfaces of disks and placed in 12-well culture plates (Costar, Corning, NY). The cell-seeded scaffolds were incubated at 37 °C in a humidified atmosphere for 4 h to make cells diffuse into and adhere to the scaffold before the addition of 3.5 mL of culture medium into each well. The cell-seeded scaffolds were replenished with fresh medium every 3 d.

Morphologies and Distributions of HDFs within Fibrous Mats. Samples were harvested on days 1, 3, and 5 after seeding, washed with phosphate buffer saline (PBS) twice, and then fixed with 4% glutaraldehyde for 2 h at 4 °C. Following three rinses with distilled water, the samples were dehydrated through a series of graded ethanol solutions and then freeze-dried. Dry constructs were sputter coated with gold and observed by SEM (Hitachi S-2700, Tokyo, Japan). To distinguish the cells from the scaffold fibers, toluidine blue staining was used for observing the cell distribution along the fibrous structure. The fixed samples were stained with 0.5 mL of freshly prepared toluidine blue solution (0.04 wt %) for 5 min at ambient temperature. Then the dye solution was washed and the slides were dehydrated before being coverslipped and observed with an inverted phase contrast microscope (Olympus BX-41, Japan). The cell-loaded fibrous scaffolds were frozen and broken under liquid nitrogen, and the infiltration of the cell into fibrous mats was detected by SEM observation of the sections. To ascertain if cells infiltrate into the scaffolds, cross-sections of cell-grown scaffolds were prepared on a cryostat (LEICA CM1900, Germany) and stained with hematoxylin and eosin. The cell infiltration was observed with the inverted phase contrast microscope.

HDF Viability Assay. Cell viability and attachment studies were determined by MTS assay (CellTiter 96, Promega, U.S.A.). On days 1, 3, and 5 after incubation, the constructs were transferred to another 24-well culture plate filled with 400 μL of fresh phenol red-free DMEM in each well. After incubating at 37 °C for 1 h, 80 μL of MTS reagent was added into each well and incubated for 4 h according to the reagent instruction. An aliquot (150 μL) of incubated medium was pipetted into a 96-well plate and placed into a microplate reader (Titertek, Helsinki, Finland), and the absorbance at 490 nm was measured for each well.

Immunohistochemistry Analysis of Cell-Grown Fibrous Mats. The relative quantity and distribution of collagen in the cell-scaffold construct is important to the properties of the seeded graft. Collagen distributions could be assessed by immunohistochemical analyses using antibodies specific to collagen type I in the scaffold.[27] Fibrous mats with cells on a 25 mm^2 coverslip were washed twice with PBS and fixed with 4% paraformaldehyde for 60 min at room temperature. The FM-LR without cell on the coverslip was used as a control. All the fixed fibrous mats were washed twice with PBS and permeabilized with 0.25% Triton X-100 in PBS at 37 °C for 15 min. Endogenous peroxidase in the cells were then blocked with 3% hydrogen peroxide in PBS for 15 min. Mouse antihuman collagen I of dilution factor 1:100 (DAKO) was applied for 2 h at 37 °C followed by incubation with rabbit antimouse secondary antibody (1:500, DAKO) for 30 min. 3,30-Diaminobenzidine (DAB) was used as a chromogenic agent, and the counterstaining was done with hematoxylin. The slides were dehydrated before coverslipped.

Statistical Analysis. All experiments were performed with $n = 4$ and the quantitative values were expressed as a mean ± standard deviation (S.D.). Whenever appropriate, two-tailed Student's t-test was used to discern the statistical difference between groups. Differences were considered statistically significant for $p < 0.05$.

Results and Discussion

Using electrospun fibers to produce tissue scaffolds shows advantages in mimicking the Ultrafine fibrils and the large network of interconnected pores of ECM of living tissues. Porosity is viewed as one of the crucial parameters for tissue engineering scaffolds. However, the electrospun mesh generally exhibits much less porosity than the conventional processing methods for tissue engineering scaffold, and it is not easy to create well-defined pore sizes through the electrospinning technique because of the randomly deposited fibers. To appropriately create the interconnected highly porous microstructure of the electrospun mesh for cell ingrowth, an innovative frame cylinder configuration was used to deposit fibers. The frame consisted of metal struts and was controlled by a stepping motor. The stepping motor was set at a very low rotation speed, which was quite different from the usual system for preparation of aligned fiber with a rotating disk.[28] It has been reported that there are two kinds of electric forces in the electrospinning process that could influence the arrangement of the electrospun fibers, namely, the electrostatic force resulting from the electric field and the Coulomb interactions between the positive charges on the nanofibers and the negative charges on the collectors.[29] When using the frame consisting of metal struts as the collector, the structure of the electric field changes and the electrostatic forces drive the fibers to move toward the metal struts. Fibers of higher density were deposited on the metal struts, while fibers of lesser density were deposited between the struts. In addition, the rotating collector would acquire much less fiber per unit time during the electrospinning process than ordinary plate collector. Both of the mechanisms presented above should increase the porosity of the fibrous mats remarkably.

Characterization of Electrospun Fibrous Mats. Figure 2 shows the fibrous morphology of electrospun mats deposited on plate collector and the rotating frame cylinder. SEM images illustrated that fibrous mats were porous, with bead-free and randomly arrayed fibers of diameters between 1.13 and 1.37 μm (Table 1). For effective cell migration, the pore sizes were expected to be no less than the HDF sizes (10−100 μm), and the link of fibers was expected to be loosening. As the whole piece of aluminum foil on the plate was used as the negative electrode, the fibrous mat deposited on plate (FM-P) layer by layer and finally formed a dense fibrous structure (Figure 2A). In contrast, fibers collected on the rotating frame cylinder were formed between the spacing of metal struts, and the connection of these fibers was not as dense as those acquired at the plate collector. Compared to the fast rotating disk or mandrel at thousands of cycles per minute, which resulted in aligned fibers,[5] large quantities of fibers randomly dispersed and laid loosely

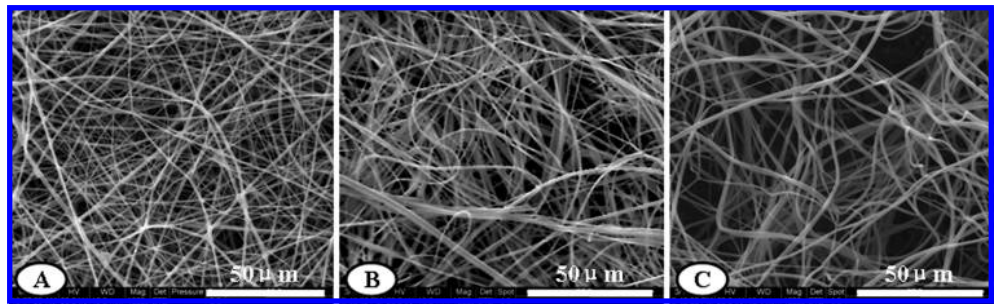

Figure 2. SEM images of electrospun fibrous mats collected on plate (FM-P, A) and the frame cylinder with rotating speed of 60 rpm (FM-HR, B) and 28 rpm (FM-LR, C).

Table 1. Characteristics of Electrospun Fibrous Mats

sample	fiber diameter (μm)	pore diameter (μm)	porosity (%)	WCA (degree)
FM-P	1.13 ± 0.12	21.0 ± 4.8	68.2 ± 3.7	131.0 ± 4.6
FM-HR	1.20 ± 0.35	59.5 ± 16.3	79.1 ± 5.2	112.4 ± 6.5
FM-LR	1.37 ± 0.28	132.7 ± 39.6	92.4 ± 4.3	76.1 ± 8.5
casting film				74.5 ± 1.3

upon each other. Large interconnected pores (voids between the fibers) formed among fibers and distributed throughout the entire fabric scaffold (Figure 2B,C).

Knowing the bulk density of the PLGA (1.25 g/cm^3), along with the calculated value of the apparent density, the porosity of the PLGA fabrics scaffold could subsequently be calculated, which is summarized in Table 1. By changing the rotation speed of the frame cylinder collector, fibrous mats with different porosities were obtained. Fibrous mats with 92.4% of porosity were obtained at the rotation speed of 28 rpm (FM-LR), and interconnected pores with an average size of 132.7 μm were dispersed in loose fibers and distributed throughout the scaffold (Figure 2C). Fibrous mats collected on cylinder with higher rotating speed of 60 rpm (FM-HR) were characterized by significantly lower porosity of 79.1% and average pore size of 59.5 μm (Figure 2B; $p < 0.05$).

The surface wettability was critical for favorable cellular responses, which should support attachment, proliferation and differentiation of cells. Many studies have demonstrated that cells adhere, spread, and grow more easily on moderately hydrophilic substrates than on hydrophobic or very hydrophilic ones.[30] The WCAs of electrospun fibrous mats and solvent casting film of PLGA are summarized in Table 1. The WCA value of the solvent casting film was only 74.5°, but much more hydrophobic surface was observed for electrospun fibrous mats of FM-P with significantly higher WCA ($p < 0.05$). During the electrospinning process, the high voltage, high speed swing and solvent evaporation may have an effect on reconstructing the chemical group distribution. Methyl groups with lower binding energy could be enriched on the fiber surface.[31] The hydrophobicity of FM-P was attributed to the combined effects of the enrichment of methyl groups on fibers surface and surface roughness of the electrospun mat itself.[32] In contrast, significant smaller values were obtained for highly porous electrospun mats ($p < 0.05$). With regard to the system of fibrous structure, various surface morphologies showed different surface roughness, which may result in different volumes of air to be trapped between interfaces of fibers and water. As the pore size among fibers increased, the surface roughness degree decreased, leading to less air entrapment in the surface pores.[33] Moderately hydrophilic FM-LR were obtained with WCA of 76.1. This was concluded that the increase in the pore size and porosity of the fabric could be favorable to improve the hydrophilicity of the fibrous mat.

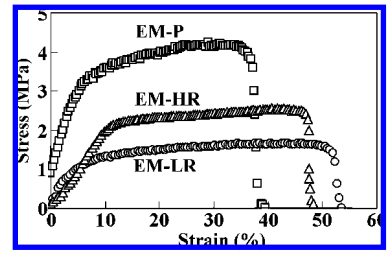

Figure 3. Stress−strain curves for electrospun fibrous mats collected on plate (FM-P), the frame cylinder with rotating speed of 60 rpm (FM-HR) and 28 rpm (FM-LR).

Scaffolds which are intended for cell culture purposes need to be robust enough for both handling and sterilization. Moreover, the scaffolds need to exhibit mechanically supportive properties for cellular morphogenesis. The strength of the fibrous mat is dependent upon inherent architecture and the bulk mechanical properties of the material.[34] To clarify the effect of porosity on the mechanical properties of electrospun fibrous mats, the uniaxial tensile strength test was conducted, and the results are shown in Figure 3. It showed that the highest tensile strength was observed for FM-P, and the tensile strength decreased with the increase in the porosity of scaffold. The ultimate tensile stress of FM-LR was 1.67 MPa, with the ultimate strain of 54.7%, which exhibited a relatively low Young's modulus but a high creep characteristic. Mechanical data on fibrous scaffold for dermal tissue engineering is limited; however, tensile strength of electrospun fibrous mats can range from 0.8 to 18.0 MPa depending on the material used.[2,25,35] Accordingly, all the scaffolds involved were found to be sufficiently durable for cell culture. On the other hand, fibrous scaffolds were not intended to be permanent replacements for native tissue, and the intrinsic material and mechanical properties of the scaffolds need not replicate that of the host environment.[15] The scaffold must simply be freestanding and capable of temporarily withstanding any forces at the injury site or during cell growth process. Thus, cell-seeded scaffolds can serve as temporary constructs for implanted cells and native cells to integrate, proliferate, differentiate, and, ultimately, regenerate the damaged tissue. Furthermore, with the cell migration into the fibrous mat, the deposition of ECM throughout the scaffold would be beneficial for the mechanical support.

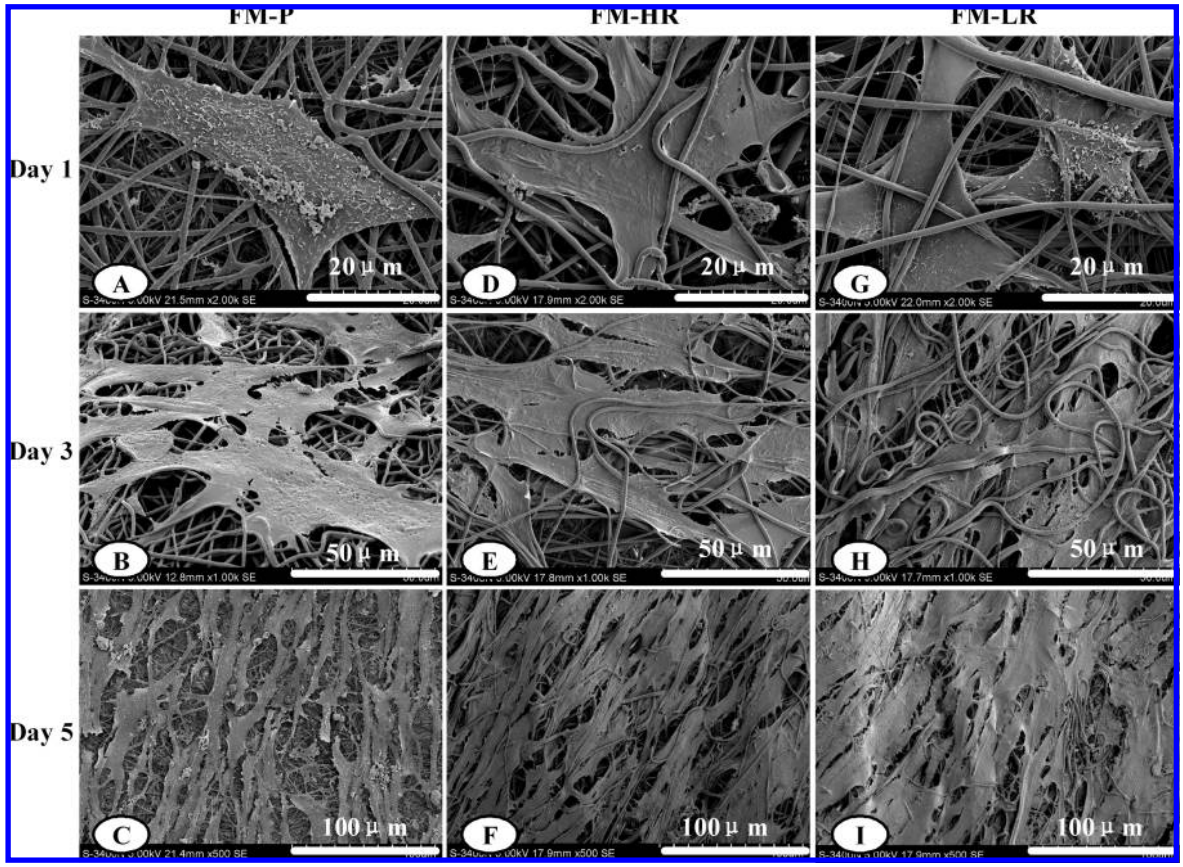

Figure 4. SEM images of cell-grown fibrous mats collected on plate (FM-P, A−C), the frame cylinder with rotating speed of 60 rpm (FM-HR, D−F) and 28 rpm (FM-LR, G−I) on days 1 (A, D, G), 3 (B, E, H), and 5 (C, F, I) after incubation.

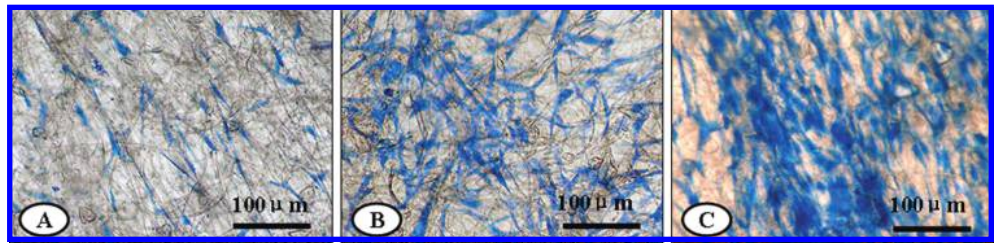

Figure 5. Images of toluidine blue-stained cells grown on fibrous mats of FM-LR after incubation for 1 (A), 3 (B), and 5 d (C).

Morphologies and Distributions of HDFs on Fibrous Scaffolds. The HDF morphology and dispersion within the fibrous mats were investigated by SEM, as shown in Figure 4. The HDF growth continued progressively on the fibrous scaffolds during the culture period. On the dense fibers collected on plate, the number of cells increased gradually and reached an estimated confluence of about 70% after a 5 d incubation (Figure 4C). Cells were shown to be spindle-shaped and distributed just on the substrate surface (Figure 4B,C). It was observed that there were few HDF infiltrations within the scaffold, and almost an HDF monolayer covered the mat. The main reason was that the pores formed in the Ultrafine fiber were still relatively small in comparison with the fibroblast with the size of 10−100 μm. In contrast, highly porous fibrous mats collected on the frame cylinder offered a 3D structure for cell infiltration and growth, as shown in Figure 4. The cells were located at the subsurface of FM-HR (Figure 4D) and even immigrated below several fibrous layers of FM-LR (Figure 4G) after a 1 d incubation. The reason was that it became easier for cells located on surface to migrate into scaffold due to the rarefaction state and high porosity of the fibrous mat. It showed that fibers crossed upon the cells and cells grew within the fibrous scaffold on day 3 after incubation (Figure 4E,H). A larger amount of cells penetrated into FM-LR of higher porosity (Figure 4H), which should be considered as a well-populated 3D scaffold. On day 5 after incubation, the cells had already increased significantly in numbers, reaching an estimated confluence of about 85% (Figure 4F,I). The confluence led to cell alignment on the surface layer and a similar profile was also observed by MacLellan et al.[36] From these experimental data, fibrous mats with higher porosity can be considered as a more suitable scaffold for fibroblast population than dense fibers.

Toluidine blue is a dye with affinity for nucleic acids and primarily used for cell staining. The dense fibers for FM-P and FM-HR prevented the light penetration through the fibrous mats, and no clear image could be collected through the inverted phase microscope. Figure 5 shows the results of toluidine blue staining, showing the direct visualization of cell adherence and distribution on the highly porous FM-LR mats at different time points. The number of the cells increased gradually in the scaffold. On days 1 and 3 after incubation, most of the cells seemed dispersal and anisotropic. But directional growth was observed on day 5 along the fibers and cells became highly confluent and were distributed on the fabric.

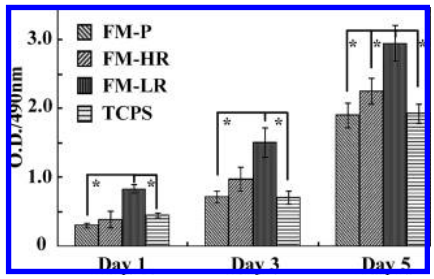

Figure 6. MTS assay of HDF growth on fibrous mats collected on plate (FM-P), the frame cylinder with rotation speed of 60 rpm (FM-HR) and 28 rpm (FM-LR). All values are an estimate of the standard uncertainty expressed as mean ± SD ($n = 4$), $*p < 0.05$.

HDF Viability on Fibrous Scaffolds. To monitor cell adhesion and viability on different substrates, the number of cells was determined by using the colorimetric MTS assay. The mechanism behind this assay was that metabolically active cells reacted with tetrazolium salt of the MTS reagent to produce soluble formazan dye that could be observed at 490 nm. The cell culture plates (TCPS) were used as control, and the results are summarized in Figure 6. It showed that HDFs cultured in all fibrous scaffolds exhibited a similar growth pattern in that cells proliferated gradually during the culture period. On days 3 and 5 after incubation, lower optical density was observed on TCPS, which was due to the 2D surface that was just suitable for the monolayer. There was no significant difference between the cell density for FM-P and that on TCPS on day 5 after incubation ($p > 0.05$). It can be concluded that cell growth on the dense FM-P is similar to that on a 2D surface. This result was also supported by the SEM data shown in Figure 4. When cells became confluent, contact inhibition resulted in the cease of mitosis. Although the overall cell number increased in all scaffolds during the culture period, the 3D and high porosity structure of PLGA fabric would offer more available space for cell migration and penetration, as well as further growth. As shown in Figure 6, the cell density on FM-LR with high porosity was significantly higher than that on FM-P at all time points ($p < 0.05$). It was also indicated that cell density on FM-LR was significantly larger than that of FM-HR on day 5 ($p < 0.05$). In conclusion, these results indicated a highly porous scaffold collected on the frame cylinder was more supportive for HDF growth.

Cross Sections of Cell−Scaffold Constructs. To ascertain cell infiltration into the inner part of the scaffold and three dimensional distribution, cross-sections were prepared and observed by SEM and optical microscope after being stained with hematoxylin and eosin. Figure 7 shows the direct visualization of the distribution and infiltration of HDFs in different fibrous mats. Please note that these photographs presented unrepresentative H&E staining. Dimethyl benzene was not used in the staining process for the clearing step because it would solve PLGA. Consequently, the polymer fabric fragments were detectable under the light microscope. In these images the black pieces and lines indicated the cross section of opaque polymer fabric fragments. It can be seen that the fabric collected on plate (Figure 7A) appeared much denser than those collected on frame cylinder (Figure 7B,C). The dense fibers were almost completely covered with a continuous HDF monolayer on the surface, but few cells infiltrated into the subsurface of fibrous mats (Figure 7A). In contrast, only a few dispersed fiber fragments remained in cross-section of the constructs composed of cells and highly porous fibrous mats, and cells had already penetrated into inner parts of the construct more than 100 μm (Figure 7B,C). The

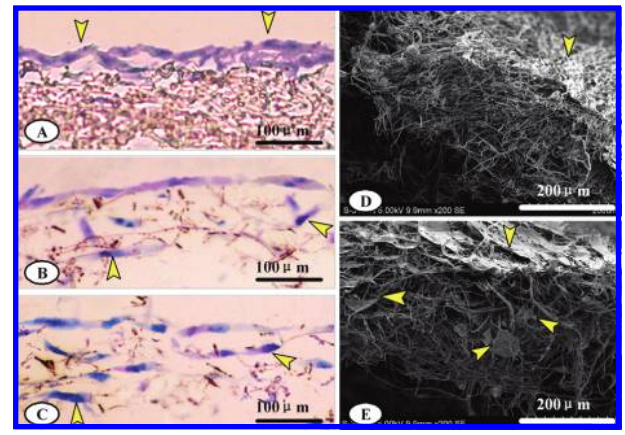

Figure 7. Cross-sections of hematoxylin and eosin stained cell-grown fibrous mats collected on plate (FM-P, A), the frame cylinder with rotation speed of 60 rpm (FM-HR, B) and 28 rpm (FM-LR, C). SEM images of cross-sections of cell-grown fibrous mats of FM-P (D) and FM-LR (E) after a 5 d incubation. Arrows indicate cells residing at the surface and inner part of the scaffold.

cell distribution pattern within the fibrous scaffolds agreed well with SEM images of cell morphology (Figure 4) and MTS analysis results (Figure 6), as described above.

The cross-sectional SEM images of FM-P and FM-LR with a thickness of about 250 μm are shown in Figure 7D,E, respectively. Cells grew into a continuous monolayer on the surface of fibrous mats, and cells infiltrated into the subsurface and inner part of the highly interconnected porous fabric. Micrographs of cross-sections of cell−scaffold constructs directly demonstrated cell migration and infiltration inside the scaffold. HDFs grown on FM-LR could be considered as the optimal cellular ingrowth.

Immunohistochemistry Analysis of Cell-Grown Fibrous Mats. One of the functions of polymer scaffolds for tissue engineering is to support the desired cellular functions and maintain phenotype-specific activities. The deposition, remodeling, and organization of the dermal ECM by HDFs are essential for tissue growth and wound healing process.[37] The adequate space inside the scaffold for cell growth and activities would lead to functional tissue regeneration. The deposition of collagen type I was tested on day 5 after incubation, and the positive staining indicated HDFs began synthesizing and accumulating collagen.[20] In the construct, which was composed of HDFs and highly porous FM-LR, the cells adhered to the fibers and spread throughout the mesh with the synthesized collagen organizing into monolayer after a 5 d culture (Figure 8C). Positive staining was also detected on cell-grown fibrous mats of FM-P and FM-HR but significantly weaker than that on FM-LR (Figure 8A,B). The results demonstrated that the highly porous scaffold not only supported cells to maintain uniform distribution but also promoted the secretion of collagen, which is the main constituent of natural ECM. It is supposed that functional scaffolds could be constructed by this elaboration and may be used for soft tissues such as skin replacement in vivo.

Conclusions

The current design for tissue engineering of a dermal substitute was that of an electrospun biodegradable scaffold through which fibroblasts could migrate and populate. A slowly rotating frame cylinder was developed as the fiber collector, and electrospun fibrous mats with porosity as high as 92.4% and average pore sizes of 132.7 μm were obtained. Higher HDF

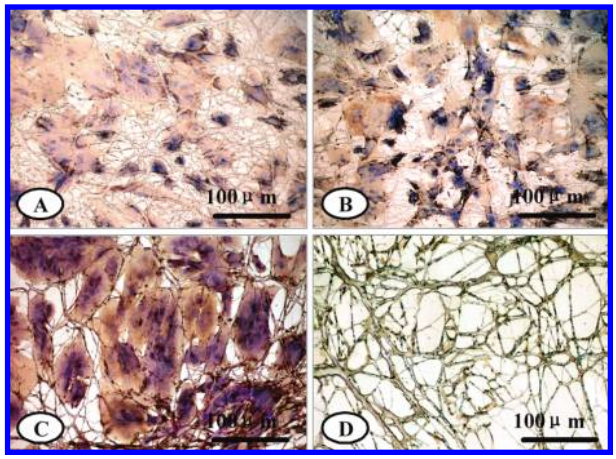

Figure 8. Immunohistochemical analyses of collagen type I of cell-grown fibrous mats of FM-P (A), FM-HR (B), and FM-LR (C) after a 5 d incubation. FM-LR without cell loading was used as control (D).

viability, collagen deposition, cell migration, and infiltration inside the scaffold were achieved for the fibrous mat with higher porosity. Maximal cellular in-growth would result in close biomimicry of the natural ECM, and the fibroblast populated 3D constructs represented the suitable characteristics of electrospun fibrous mats with high porosity to build up a scaffold for skin tissue engineering.

Acknowledgment. This work was supported by National Natural Science Foundation of China (20774075), Program for New Century Excellent Talents in University (NECT-06-0801), and Fok Ying Tong Education Foundation (104032), Ministry of Education of China.

References and Notes

(1) Pham, Q. P.; Sharma, U.; Mikos, A. G. *Tissue Eng.* **2006**, *12*, 1197.
(2) Barnes, C. P.; Sell, S. A.; Boland, E. D.; Simpson, D. G.; Bowlin, G. L. *Adv. Drug Delivery Rev.* **2007**, *59*, 1413.
(3) Li, W. J.; Laurencin, C. T.; Caterson, E. J.; Tuan, R. S.; Ko, F. K. *J. Biomed. Mater. Res.* **2002**, *60A*, 613.
(4) Xin, X.; Hussain, M.; Mao, J. J. *Biomaterials* **2007**, *28*, 316.
(5) Xu, C. Y.; Inai, R.; Kotaki, M.; Ramakrishna, S. *Biomaterials* **2004**, *25*, 877.
(6) Zong, X. H.; Bien, H.; Chung, C. Y.; Yin, L. H.; Fang, D. F.; Hsiao, B. S.; Chu, B.; Entcheva, E. *Biomaterials* **2005**, *26*, 5330.
(7) Schnell, E.; Klinkhammer, K.; Balzer, S.; Brook, G.; Klee, D.; Dalton, P.; Mey, J. *Biomaterials* **2007**, *28*, 3012.
(8) Murugan, R.; Ramakrishna, S. *Tissue Eng.* **2006**, *12*, 435.
(9) Lee, J. J.; Lee, S. G.; Park, J. C.; Yang, Y. I.; Kim, J. K. *Curr. Appl. Phys.* **2007**, *7*, 37.
(10) Eichhorn, S. J.; Sampson, W. W. *J. R. Soc. Interface* **2005**, *2*, 309.
(11) Zong, X.; Kim, K.; Fang, D.; Ran, S.; Hsiao, B. S.; Chu, B. *Polymer* **2002**, *43*, 4403.
(12) Van Lieshout, M. I.; Vaz, C. M.; Rutten, M. C.; Peters, G. W.; Baaijens, F. P. *J. Biomater. Sci., Polym. Ed.* **2006**, *17*, 77.
(13) Kidoaki, S.; Kwon, I. K.; Matsuda, T. *Biomaterials* **2005**, *26*, 37.
(14) Nam, J.; Huang, Y.; Agarwal, S.; Lannutti, J. *Tissue Eng.* **2007**, *13*, 2249.
(15) Chiu, J. B.; Liu, C.; Hsiao, B. S.; Chu, B.; Hadjiargyrou, M. *J. Biomed. Mater. Res.* **2007**, *83A*, 1117.
(16) Pham, Q. P.; Sharma, U.; Mikos, A. G. *Biomacromolecules* **2006**, *7*, 2796.
(17) Chong, E. J.; Phan, T. T.; Lim, I. J.; Zhang, Y. Z.; Bay, B. H.; Ramakrishna, S.; Lim, C. T. *Acta Biomater.* **2007**, *3*, 321.
(18) Li, Y.; Ma, T.; Kniss, D. A.; Lasky, L. C.; Yang, S. T. *Biotechnol. Prog.* **2001**, *17*, 935.
(19) Laurencin, C. T.; Ambrosio, A. M.; Borden, M. D.; Cooper, J. J. *Ann. Biomed. Eng.* **1999**, *1*, 19.
(20) Pan, H.; Jiang, H.; Chen, W. *Biomaterials* **2006**, *27*, 3209.
(21) Deng, X. M.; Xiong, C. D.; Cheng, L. M. *J. Polym. Sci., Part C: Polym. Lett.* **1990**, *28*, 411.
(22) Cui, W. G.; Li, X. H.; Zhu, X. L.; Yu, G.; Zhou, S. B.; Weng, J. *Biomacromolecules* **2006**, *7*, 1623.
(23) Cui, W. G.; Li, X. H.; Zhou, S. B.; Weng, J. *J. Appl. Polym. Sci.* **2007**, *103*, 3105.
(24) Oh, S. H.; Park, I. K.; Kim, J. M.; Lee, J. H. *Biomaterials* **2007**, *28*, 1664.
(25) He, W.; Ma, Z. W.; Yong, T.; Teo, W. E.; Ramakrishna, S. *Biomaterials* **2005**, *26*, 7606.
(26) Huang, S.; Deng, T. Z.; Wang, Y. J.; Deng, Z. H.; He, L. S.; Liu, S. X.; Yang, J. J.; Jin, Y. *Acta Biomater. Doi:*. **2008,** 10.1016/j.actbio.2008.02.007.
(27) Stitzel, J.; Liu, J.; Lee, S. J.; Komura, M.; Berry, J.; Soker, S.; Lim, G.; Van Dyke, M.; Czerw, R.; Yoo, J. J.; Atala, A. *Biomaterials* **2006**, *27*, 1088.
(28) Katta, P.; Alessandro, M.; Ramsier, R. D.; Chase, G. G. *Nano Lett.* **2004**, *4*, 2215.
(29) Li, D.; Xia, Y. N. *Adv. Mater.* **2004**, *16*, 361.
(30) Wang, Y. Q.; Cai, J. Y. *Curr. Appl. Phys.* **2007**, *7*, 108.
(31) Deitzel, J. M.; Kosik, W.; McKnight, S. H.; Beck-Tan, N. C.; DeSimone, J. M.; Crette, S. J. *Polymer* **2002**, *43*, 1025.
(32) Ma, M.; Hill, R. M.; Lowery, J. L.; Fridrikh, S. V.; Rutledge, G. C. *Langmuir* **2005**, *21*, 5549.
(33) Cui, W. G.; Li, X. H.; Zhou, S. B.; Weng, J. *Polym. Degrad. Stab.* **2008**, *93*, 731.
(34) Baker, S. C.; Atkin, N.; Gunning, P. A.; Granville, N.; Wilson, K.; Wilson, D.; Southgate, J. *Biomaterials* **2006**, *27*, 3136.
(35) Duan, B.; Yuan, X. Y.; Zhu, Y.; Zhang, Y. Y.; Li, X. L.; Zhang, Y.; Yao, K. D. *Eur. Polym. J.* **2006**, *42*, 2013.
(36) Heydarkhan-Hagvall, S.; Schenke-Layland, K.; Dhanasopon, A. P.; Rofail, F.; Smith, H.; Wu, B. M.; Shemin, R.; Beygui, R. E.; MacLellan, W. R. *Biomaterials* **2008**, *29*, 2907.
(37) *The molecular and cellular biology of wound repair*, 2nd ed.; Clark, R. A. F., Ed.; Plenum: New York, NY, 1996; pp 3−35.

BM800476U